Full Length Article

Theoretical insights into the behaviors of sodium and aluminum on the cathode titanium diboride surfaces

Chaohong Guan, Hong Zhu [*]

University of Michigan–Shanghai Jiao Tong University Joint Institute, Shanghai Jiao Tong University, Shanghai 200240, China

A B S T R A C T

Density functional theory calculations were adopted to systematically investigate the adsorption and diffusion behaviors of sodium and aluminum over TiB$_2$ surfaces or in TiB$_2$ crystal to characterize the interaction mechanism between sodium and TiB$_2$ cathode in aluminum reduction cells. Results suggest that Na and Al will stably adsorbe on the low-index TiB$_2$ (0 0 0 1) surface, and the presence of vacant defects can significantly strengthen this adsorption. The migration of Na and Al over pristine TiB$_2$ is anisotropic, with the largest energy barrier of 0.024/0.32 eV for Na and 0.28/1.57 eV for Al over Ti/B-terminated surfaces. The Ti vacancy in Ti-terminated surface is more effective to hinder Na and Al migration with the large diffusion barriers of 0.36 eV for Na and 2.07 eV for Al. Specially, for the B-terminated surface, B vacancy will promote the Na and Al diffusion with the lower barriers. Additionally, it is difficult for Na and Al to form interstitial defects and diffuse in covalent TiB$_2$ crystal. Given these results, compared to graphite cathode, the sodium prefers to deposit on TiB$_2$ surface, and the strong interaction between sodium and TiB$_2$ promotes the early process of sodium penetration. On the other hand, the smoother landscape for Na diffusion on the TiB$_2$ surface suggests the decreased stability of aluminum liquid, so that the current efficiency of aluminum reduction cell will decrease.

1. Introduction

Intense research efforts have been devoted to the development of the high-energy-efficient and environment-friendly aluminum reduction cells. However, with the poor wettability towards aluminum, the metal pad fluctuates, a thick aluminum liquid layer and a large anode-cathode distance must be maintained, leading to the high energy consumption during aluminum electrolysis process. More recently, inert and wettable cathodes have attained increased attention from the cathode development community due to the elimination of magnetohydronamic disturbances in the metal pad. This may allow for smaller anode-cathode distances, leading to reduced energy consumption and potentially extending the lifetime of cathode and aluminum electrolysis cell. Many attempts [1,2] have been made to rigorously explore and develop various new cathode materials, such as TiB$_2$, TiC, ZrC, etc. Among these materials, titanium diboride has received tremendous attentions and been regarded as the most suitable material for next-generation wettable cathode [3,4], attributing to the perfect wettability with liquid aluminum.

However, the implementation of new cathodes is not straight

forward, mainly due to the challenge of understanding the mechanisms that cause the cathodes to fail [5]. To the best of our knowledge, during the aluminum reduction process in Hall-Heroult cell, not only aluminum but also sodium will precipitate on the cathode materials surface, sodium reacts with and penetrates into cathode materials at the electrolysis temperature of 940℃~970℃, causing the significant changes in physical, mechanical and chemical properties of cathode [6,7]. As a result, the cathode degrades and the cell shutdowns prematurely [8,9]. Recently, numerous efforts have been made to explore the diffusion or penetration mechanisms of sodium in traditional cathodes. Most researchers [10,11] agree with the opinion that sodium vapor diffuse into cathode materials by the hole channels of carbon surface. Intriguingly, the study of Dewing [12] claims sodium will penetrate into the crystal lattice or grain boundaries of the cathode materials, and the diffusion rate is very fast with the diffusion coefficient of $1 \times 10^{-5} \sim 5 \times 10^{-5}$ cm^2/s. It is worth mentioning that carbon-based materials are adopted as the conventional cathodes for aluminum reduction cell and sodium can accelerate its degradation [13,14]. In this regard, early studies reported [15,16] sodium atoms penetrate into graphite layers and interact with carbon, then forming the thin intercalation compounds, which

attributes to the charge transfer between metal atom and carbon π bond [17]. Brilloit et al. [18] reported that the intercalation compounds may be the C_{60}Na or C_{68}Na, while Matuyama [19] and Nafaa et al. [20] suggested that the liquid sodium reacts with graphite and forms C_{64}Na, the layer spacing of which is 3.5 Å (pure graphite is 3.34 Å [21]). Titanium diboride, as the next-generation wettable cathode, its performance against the sodium penetration has obtained increasing concerns but still needs further investigation [22]. Xue and H.A. Oye [23] reported that TiB_2 material can limit the sodium penetration, whereas improve the wetting property between Al liquid and cathode. However, Wang et al. [24] investigated the stability of TiB_2 when exposed to Na environment and indicated the TiB_2 material showed surprisingly high reactivity with sodium. Hence, it seems to be inevitable that sodium atoms penetrate and diffuse into TiB_2 composites through surface holes or carbon grain boundaries, resulting in the damage and failure of cathode. However, there are few studies focused on the damage mechanisms of TiB_2 in Na-rich environment, which impedes the development of novel TiB_2 wettable cathode.

In addition, prior theoretical studies [25] report that sodium is energetically unstable to be attracted to the surface than to be intercalated in the interlayer of graphite, and the energy barriers for sodium diffusion range from 0.09 eV to 0.16 eV for different migration pathways [26]. The presence of defects [27,28] can effectively enhance the adsorption of sodium on graphite, such as mono-vacancy, divacancy and stone-wales defects [25], which shows relatively larger energy barriers for sodium diffusion (0.58 eV, 0.95 eV and 0.55 eV, respectively). Meanwhile, they suggested that the energy barrier for sodium migration process in the interlayer (0.32 eV) is larger than that on the pristine graphite surface, while the defects will promote the sodium diffusion process with the lower barriers (0.15 eV) along the Stone-Wales defects in the graphite interlayer. Hence, sodium will penetrate into and degrade the graphite-based cathode. For the next-generation wettable TiB_2 cathode, however, the high temperature and strong corrosive atmosphere make it is difficult to experimentally investigate its damage mechanism and presently there is no theoretical exploration of sodium adsorption or migration on it, which severely hinders the development of wettable cathode materials.

Therefore, in the present work, we applied first-principles calculations based on density functional theory (DFT) to gain a theoretical insight into the interactive behaviors between titanium diboride cathode material and sodium. Our prime focus is to understand sodium adsorption and diffusion mechanism on TiB_2, which will be compared with the adsorption and diffusion behaviors of aluminum (Al). Firstly, the surface energies of pristine TiB_2 (0 0 0 1) surfaces and the formation energies of Ti vacancy (V_{Ti}) and B vacancy (V_B) were calculated. Then, the favorable adsorption sites for Na and Al over Ti-terminated and B-terminated surfaces were identified, and then the influences of Ti and B vacancies on the adsorption of Na and Al were considered, respectively. Additionally, the projected density of states (PDOS) and charge density difference analysis were adopted for the insights of Na and Al adsorption behaviors. Finally, the linear synchronous (LST) and quadratic synchronous transit (QST) methods were performed to search the minimum energy pathways (MEPs) [29] and energy barriers for Na and Al diffusion on TiB_2 surfaces or in TiB_2 crystal.

2. Computational methods

Plane-wave-based spin-polarized [30] DFT calculations were adopted using the Perdew-Burke-Ernzerhof (PBE) [31] exchange-correlation functional within the generalized gradient approximation (GGA), and the CASTEP package was employed in this work.[32,33] The atomic positions for surface and bulk TiB_2 were optimized with the cutoff energy of 500 eV and 700 eV, respectively, the lattice constant of bulk TiB_2 was also optimized. In addition, to avoid the image interaction due to periodicity, a vacuum layer of 15 Å was added along the z direction of TiB_2 surface.[34] During structural optimization, the total energy

convergence criteria is 5.0×10^{-6} eV/atom, and the force convergence criteria is 0.01 eV/Å. The Brillouin zone was sampled by Monkhorst-Pack grids [35] of $13 \times 13 \times 13$ for the unit cell and $3 \times 3 \times 1$ for the surface slab model. The TiB_2 surface was modeled by a periodic slab containing five atomic layers with 63 atoms, whereas the vacancies were considered. When calculating the adsorption energies of sodium over pristine and defective TiB_2 surface, the Grimme dispersion correction (D2) [36,37] is taken into account so as to resolve the van der Waals interaction. To confirm the most favorable adsorption positions, sodium atom was placed above the TiB_2 surface at different sites, followed by structural optimization. And the adsorption energy (E_{ad}) is calculated to determine the most favorable site [38]. A negative value illustrates that the adsorption is energetically stable and spontaneous. Additionally, the LST/QST method [39] was performed to simulate the sodium-ion diffusion and gain the associated energy barriers.

The surface energy γ is also determined to characterize the stability of a particular crystal facet, which measures the work required to create the facet from the crystal [40]. Further, the formation energy for vacancy on the surface of TiB_2 could be calculated based on the following equation.

$$E_f = E_{defect} - E_{pristine} + \sum_i N\mu_i$$

The E_{defect} and $E_{pristine}$ represent the total energy of the defective and the pristine surface respectively, N is the number of atoms removed from the pristine surface to create defects, and μ_i is the chemical potential of the removed atoms in the stable bulk state.

3. Results and discussion

3.1. Structure of pristine and defective TiB_2 surface

To validate our simulations, we compare the optimized TiB_2 unit cell with a = 3.029 Å, b = 3.029 Å and c = 3.18 Å (Fig. 1a) to the already reported results. Wang and co-workers [41] reported a DFT calcuated lattice constant of a = 3.034 Å, b = 3.034 Å and c = 3.224 Å. Burdett et al.[42] and Topor et al.[43] experimentally reported lattice constants of a = 3.032 Å, b = 3.032 Å and c = 3.229 Å. The TiB_2 (0 0 0 1) surfaces as the representative surfaces [44,45] are considered in this work. The two possible terminations for TiB_2 (0 0 0 1) surfaces, i.e., Ti-terminated and B-terminated surfaces (Fig. 1b and c), have the surface energies of 2.25 J/m^2 and 2.36 J/m^2, respectively, which are in excellent agreement with previous studies [46]. With the increased $\mu_B^{slab} - \mu_B^{bulk}$ the surface energy of Ti-terminated surface increases, while the energy of B terminated decreases, and the former surface is thermodynamically more favorable when $\mu_B^{slab} - \mu_B^{bulk}$ is less than −0.72 eV. Oppositely, the B-terminated surface is thermodynamically more favorable.

For Ti- and B-terminated TiB_2(0 0 0 1) surface, a Ti vacancy (V_{Ti}) and a B vacancy (V_B) can be introduced, respectively (Fig. 1f and g). The formation energies for V_{Ti} and V_B are 2.38 and 3.51 eV under Ti-rich condition, and 5.44 and 2.55 eV under B-rich condition, respectively (Fig. 1d). In general, the V_{Ti} under Ti-rich condition is more likely to form in the surface with the lowest formation energy.

3.2. Adsorption of Na on pristine and defective TiB_2 (0 0 0 1) surface

Cathodic sodium penetration for electrolysis cell is generally considered to involve the following processes: (1) sodium atoms initially adsorb, diffuse on the cathodic surface; (2) and then cross the surface and penetrate into the bulk. Hence, we first examined the sodium adsorption behaviors on the TiB_2 (0 0 0 1) surface to reveal their interaction mechanisms. Based on the previous work [47] about W adsorption on pristine TiB_2 surface, we considered several possible adsorption sites in this work (Fig. 1b and c), which include (1) the top site of Ti (B) atom, (2) the hollow site formed by three Ti atoms (six B
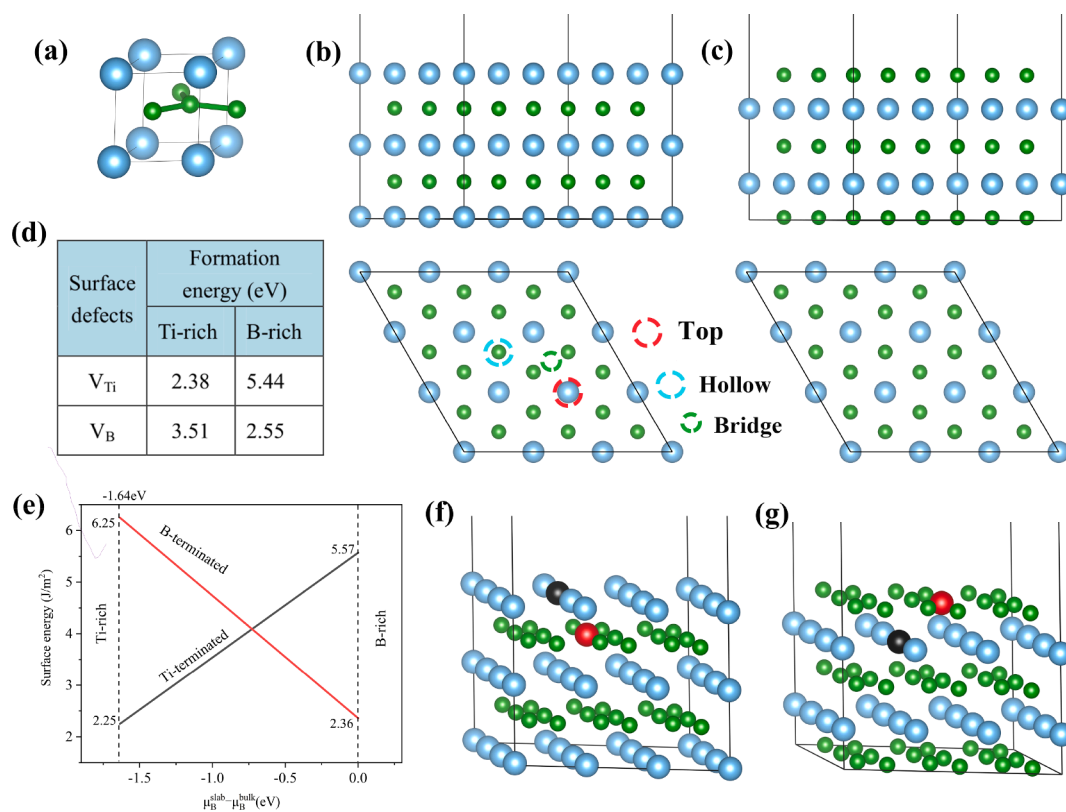
Fig. 1. (a) The optimized unit cell of TiB$_2$. (b) the side view and (c) the top view of the Ti-terminated and B-terminated surfaces, respectively. (d) Formation energies associated with the surface vacancies under both Ti-terminated and B-terminated conditions. (e) Surface energies of TiB$_2$(0 0 0 1) surfaces with Ti termination and B termination as a function of the B chemical potential. (f) and (g) are the optimized Ti-terminated and B-terminated surfaces with Ti vacancy and B vacancy, respectively. The black sphere represents the Ti vacancy, and the red sphere represents the B vacancy.

atoms), and (3) the bridge site of Ti (B) atoms of Ti-terminated (B-terminated) surfaces. The relaxed structures for these adsorption calculations are shown in Fig. S1. The adsorption energies of Na over different sites are shown in Table 1. The negative adsorption energies for all the adsorption sites suggest that the sodium deposition on the TiB$_2$ (0 0 0 1) surface is a spontaneous process, which is an essential requirement for sodium penetration.

For both Ti-terminated and B-terminated surfaces the hollow site is the most favored site for Na adsorption with the adsorption energies of −2.49 and −3.87 eV, respectively. The previous reports [48,49] have suggested that the hollow site of graphite is the most energetically favored site for sodium adsorption with the adsorption energies of −0.71

or −0.67 eV, which is lower than that of Ti-terminated and B-terminated surfaces of TiB$_2$. Thus, the sodium atoms are more likely to accumulate on Ti/B-terminated surface than graphite surface (causing the more serious sodium deposition than graphite cathode and reducing the stability of electrolyte), which may promote the next penetration process. The corresponding charge density differences (CDD) of Na adsorption over the hollow-site are presented in Fig. 2 and the CDD of Na adsorption over top and bridge sites are presented in Fig. S2. For Ti-terminated surface, charge accumulation takes place between Na atom and Ti atoms while charge depleted regions surround the Na and Ti atoms, indicating that strong covalent Na-Ti bonds are formed after Na adsorption. Additionally, for the Na adsorption over the B-terminated surface, strong ionic Na-B bond is formed and the charge accumulation occurs around B atoms while charge-depleted regions surround the Na atom, suggesting the net charge transfer from the Na atom to TiB$_2$. To quantify the amount of charge transfer during adsorption process, Hirshfeld charge analysis [50] was also carried out. The results show that over hollow sites, the charged state of Na atoms are +0.33|e| and +0.52|e| for Ti-terminated and B-terminated surfaces, respectively, showing Na adsorption over B-terminated surface is more energetically favorable.

Meanwhile, the Al adsorbs on TiB$_2$ surfaces was also considered and the associated adsorption energies are listed in Table 1. Similar to Na adsorption, the hollow site is the most stable site for Al adsorption with the largest adsorption energies of −4.07 eV and −6.23 eV on the Ti-terminated and B-terminated surfaces, respectively. Obviously, Al adsorption over B-terminated surface is more energetically favorable and the wettability between Al and TiB$_2$ surfaces is better than Na element. Despite this, the negative adsorption energy of Na suggests the large possibility for the deposition of Na on the TiB$_2$ surface under Na-rich environment, which is detrimental to the stability for cell operation.
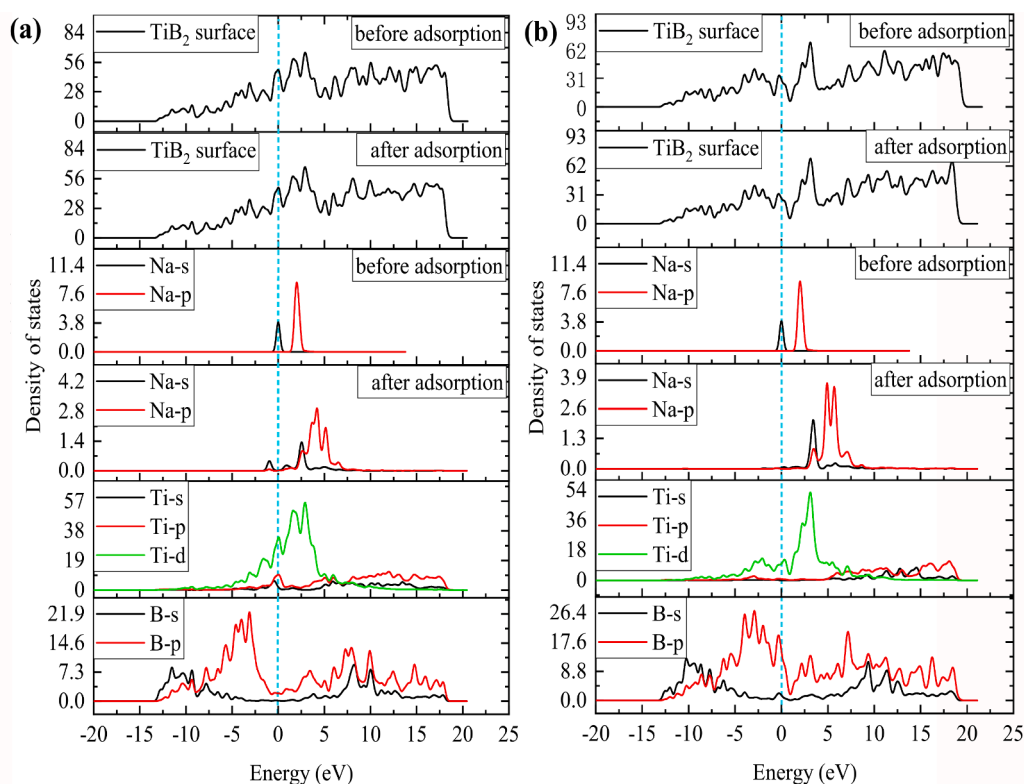
Table 1
The adsorption energy (E_{ad}, eV) and the distance (d, Å) between sodium atom and the outermost layer of TiB$_2$ (0 0 0 1) surfaces.

Surface type		Pristine TiB$_2$ surface			V$_{Ti}$	V$_B$
		Top	Hollow	Bridge		
Ti-terminated						
Na adsorption	E_{ad}	−2.393	−2.491	−2.48	−2.90	−2.52
	d	2.883	2.683	2.721	0.768	2.685
Al adsorption	E_{ad}	−3.49	−4.07	−3.92	−5.67	−4.21
B-terminated						
Na adsorption	E_{ad}	−3.407	−3.87	−3.42	−3.48	−3.55
	d	2.375	2.087	2.317	2.102	1.76
Al adsorption	E_{ad}	−4.65	−6.23	−4.67	−5.78	−5.8
Graphite	E_{ad}	−0.655	−0.71 [48], −0.67 [49]	−0.664	–	–

Fig. 2. Total density of states before and after sodium adsorption, and the projected density of states (PDOS) of the Na bounded to the hollow site of (a) Ti-terminated and (b) B-terminated surfaces. The light blue dotted lines represent the Fermi level, which were set to 0 eV.

Previous studies [51,52] have reported that the defective zone can promote the adsorption of metal adatoms due to the dangling bonds. To explore the influence of defects on the Na adsorption, the V_{Ti} and V_B defects were considered in our work, the corresponding optimized Na adsorption configurations are shown in Fig. S1. On Ti-terminated surface, Na atom prefers to get adsorbed at the V_{Ti} site with the most negative adsorption energy of −2.9 eV (Table 1), and the B vacancy also promotes the Na adsorption with the relatively more negative adsorption energy of −2.52 eV compared to the pristine surface. While, in the case of B-terminated surface, the adsorption energies for Na over the V_{Ti} and V_B sites are −3.48 and −3.55 eV, respectively, which are higher than that for Na adsorption over the hollow site of pristine surface. Therefore, the defects in Ti-terminated surface strengthen the interaction between sodium and TiB_2 surface and accelerate the sodium penetration. Charge density difference for Na adsorption over defective TiB_2 surfaces are presented in Fig. S2, suggesting the strong covalent or ionic bonds formed between Na atom and Ti or B atoms. On the other hand, the vacant defects also enhance the bonding between Al and TiB_2 surfaces. The adsorption energies are −5.67, −4.21 eV for Al over V_{Ti} and V_B sites of the Ti-terminated surface, while for V_{Ti} and V_B sites in B-terminated surface, the corresponding adsorption energies are −5.78 and −5.8 eV, respectively.

The projected density of states (PDOS) for the most stable sodium adsorption sites (Hollow site) were performed to better understand the adsorption mechanism and the electronic structures, as shown in Fig. 2 (the PDOS of Na adsorption over defective TiB_2 surface are presented in Fig. S3). For most adsorption systems, compared to the pristine TiB_2 surfaces, DOS of TiB_2 surfaces after Na adsorption are similar: the positions of peaks are almost the same, indicating that the electronic properties of TiB_2 surfaces won't be affected by sodium adsorption. However, for the sodium adsorption over Ti-terminated surfaces, strong hybridization can be observed between sodium atom and TiB_2 surfaces, suggesting the large adsorption energies observed. Moreover, the strong binding energies are attributed to the hybridization between Na-s, p

orbitals and Ti-d orbitals, B-s,p orbitals near the Fermi level.

Compare to the PDOS of sodium before adsorption, the corresponding peaks of sodium shift toward the higher energy for all adsorption systems so that the metal s, p-states are unoccupied in the conduction band, suggesting that the sodium atom donates electron to the surface, consistent with the Hirshfeld charge analysis. It can be seen that the Na 2s states located at 2.5 eV and 3.4 eV above the Fermi level for Na adsorption over Ti-terminated and B-terminated surfaces, respectively, which further demonstrates that Na adsorption over B-terminated surface is energetically more favorable than Ti-terminated surface as it is more difficult to revert to its atomic state. Correspondingly, for the vacant defects of Ti-terminated surface, the Na 2s states lie at 3.03 eV and 2.52 eV for Na adsorption over V_{Ti} and V_B sites, respectively, meaning that the Ti-vacant defects strengthen the adsorption of Na atoms and promote the sodium corrosion in a greater degree than B-vacant defects in this terminated surface. On the contrary, the B vacancy is more effective to promote the sodium corrosion for the B-terminated surface (the Na 2s states locate at 3.12 eV and 3.32 eV for Na adsorption over V_{Ti} and V_B sites of B-terminated surface).

3.3. Sodium diffusion on TiB_2 surface

The performance of TiB_2 cathode is significantly affected by the interactions between sodium and TiB_2 surface, and the sodium penetration relies upon the adsorption and mobility of the sodium atoms over the cathode. The mobility is determined by the diffusion barrier associated with the transport of the atom, where the smaller energy barrier facilitates faster atomic diffusion. To further study the sodium behavior on TiB_2 surface, the LST/QST method was performed to confirm the transition states and energy barriers.

As discussed earlier, differences in the adsorption energies of Na over Hollow sites and Bridge sites are minimal for the Ti-terminated surface, and adatom will diffuse over the surface by hopping from the Hollow site to its nearest neighbors. Herein, to find the minimum energy pathways

(MEPs) for Na diffusion, four distinct pathways were investigated according to the symmetries of Ti-terminated surface. As shown in Fig. 3a, these paths are: path H1 → H2 (P1), path H2 → Top → H3 (P2), B1 → Top → B2 (P3), and path B1 → B2 (P4). Specially, P1 and P2 were considered for Al diffusion on Ti-terminated surface. Similarly, the MEPs and the energy barriers of Na/Al diffusion on B-terminated surface are presented in Fig. 4b, three pathways were investigated including the path H1 → Top → H2 (P5), path H1 → Bridge → H2 (P6) and path H3 → H4 (P7). The energy profiles displayed on the left and right panels of Fig. 3 represent the energy barriers of Na and Al diffusions, respectively.

Considering the Ti-terminated surface, the energy barriers for Na and Al diffusion along P1 are 0.005 and 0.16 eV, respectively. Hopping from a H1-site to the next H2-site will across a metastable bridge site, hence, two transition states appear for Na diffusion in this case, which attributes to the structural symmetry and the minimum adsorption energy difference for Na on the hollow and bridge sites. In comparison, the energy required for the diffusion along P2 path is relatively higher for both Na and Al atoms. In this path, atom will migrate over the top of Ti atom and the energy barrier is 0.023 and 0.28 eV for Na and Al diffusion. On the other hand, the migration from one bridge (B) site to another bridge site for Na diffusion will occur as either P3 or P4, and the corresponding energy barriers are 0.005 and 0.024 eV. In short, on the Ti-terminated surface, diffusion of Na and Al is anisotropic and diffusion along the P1 path is faster than along the P2 path. And the energy barriers corresponding to the diffusion of Na are smaller than those for Al which implies that Na would diffuse faster than Al on Ti-terminated surface. Interestingly, the energy barrier of Na diffusion on graphite surface is 0.1 eV, which is larger than that of Na on Ti-terminated surface, indicating that Na moves easily on the Ti-terminated surface.

For the B-terminated surface, Al atoms also have the higher diffusion barriers than Na atoms (Fig. 3b). For Na diffusion, the energy barriers for the P5, P6 and P7 paths are around 0.3–0.32 eV, which are larger than those over the Ti-terminated surface. Additionally, the energy barriers for Al migration along P5, P6 and P7 path are 1.57, 1.50 and 1.57 eV, which are larger than that of Na. Therefore, Na atoms would diffuse faster than Al on B-surface and the P6 path is the most preferred migration path for both Na and Al atoms. Also, it is obvious that the diffusion of Na and Al are faster on the Ti-terminated surface than that on the B-terminated surface due to the lower energy barriers.

The introduction of surface vacancy will boost the adsorption energies for Na and Al atoms on TiB_2 surface, while the defective sites sometimes essentially act as traps and inhibit the atomic motion in this case. For the defective TiB_2 surfaces, we have simulated the migration of Na and Al atoms from the defective regions, including the V_{Ti} and V_B of the Ti-terminated and B-terminated surfaces, and the MEPs and associated energy profiles for Na/Al diffusion are displayed in Fig. S4. Our LST/QST simulations for Na and Al diffusion suggest that V_{Ti} and V_B trap the both atoms and as a result the energy barriers are increased compared to the pristine surfaces. For the Ti-terminated surface, the energy barriers for escaping the V_{Ti} defective site are larger than that of V_B defective sites. As shown in Fig. S4a, for Na and Al diffusion on V_{Ti} surface, the barriers for path V → H1 (P8) and V → Top → H1 (P9) are 0.36, 0.25 eV and 2.06, 2.07 eV, respectively. It is obvious that Na prefers to diffusing along P8 and the Ti vacancy will severely limit Na and Al diffusion. Similarly, for V_B surface (Fig. S4b), we also considered two migration paths, namely, VB → H1 (P10) and VB → H3 (P11). The barriers for Na and Al diffusion along P10 and P11 are 0.019, 0.036 eV and 0.19, 0.32 eV, respectively, which are slightly larger than that for Na and Al migration on pristine Ti-terminated surface, and this phenomenon is attributed to the little change of adsorption energies for different sites. Hence, for the Ti-terminated surface, it can be concluded that Ti vacancy is more effective to hinder the Na and Al migration and hence contributes to the stability of aluminum liquid layer.

On the other hand, exploring the effects of Ti vacancy of B-terminated surface on atomic diffusion (Fig. S4c), two migration pathways were considered, namely, path H4 → H3 (P12) and H4 → VTi (P13), the associated energy barriers are 0.36, 0.33 eV for Na, and it would diffuse faster along P13 than P12. Whereas, due to the relatively greater difference in adsorption energy of Al atoms on the V_{Ti}, Bridge and Top adsorption sites than the Na atoms, Al atoms will be slower and the
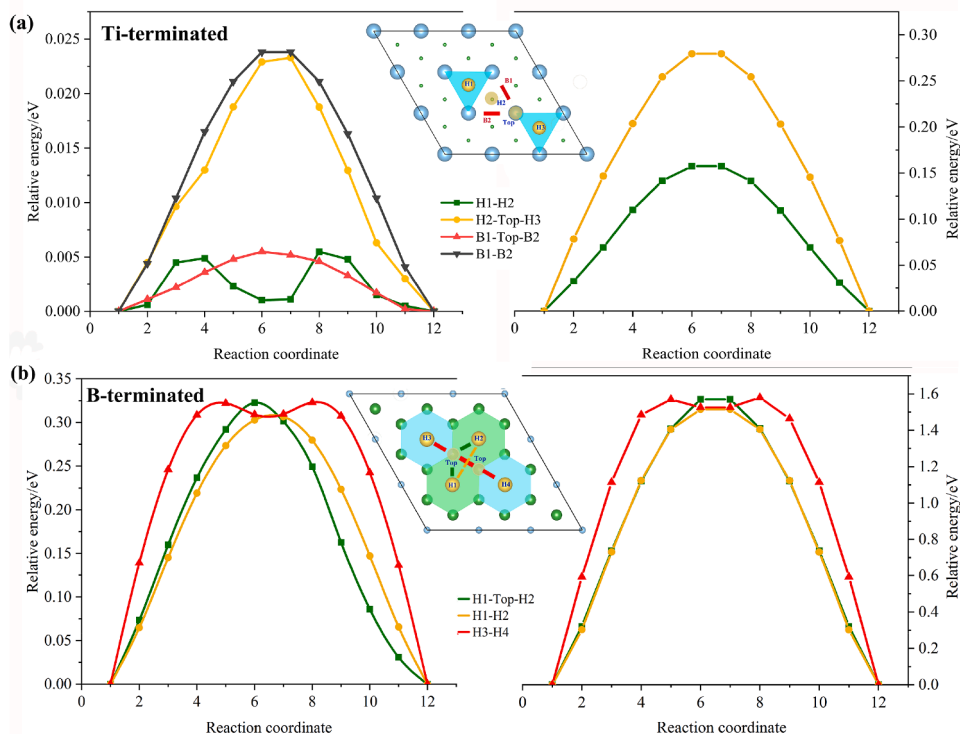

Fig. 3. Different diffusional pathways and associated energy barriers for the diffusion of Na (left) and Al (right) atoms over pristine (a) Ti-terminated and (b) B-terminated surfaces. H, Top and B represent the center, top and bridge sites of Ti or B atoms on the Ti/B-terminated surfaces.
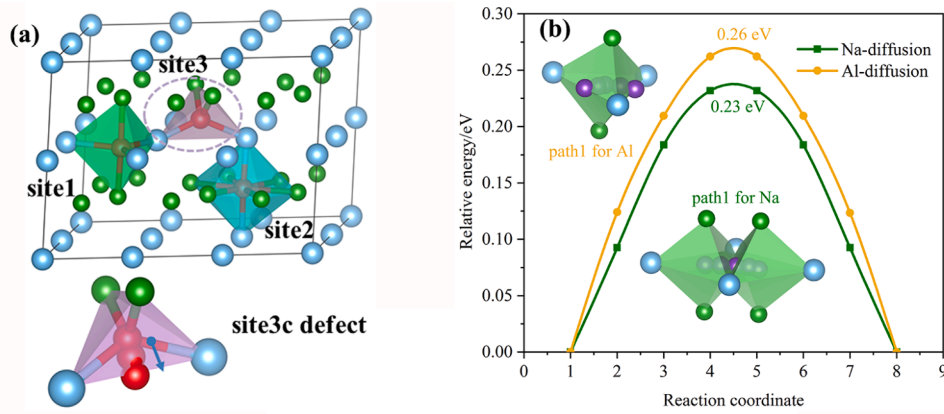
Fig. 4. (a) Three possible defective sites for Na and Al in TiB$_2$ crystal, site3c suggests that the Na/Al interstitial defects in site3 are unstable.

migration barriers for paths P12 and P13 are 1.58 and 1.66 eV, respectively. For V$_B$ surface, as shown in Fig. S4d, the energy barriers of path H4 → H3 (P14) and H4 → VB → H1 (P15) are 0.28, 0.015 eV for Na and 1.3, 0.33 eV for Al, of which the Na or Al diffuse faster along P15. From these values of diffusion energy barriers, it is clear that the B vacancy of B-terminated surface will promote the Na and Al diffusion, which is obviously detrimental to the stability of aluminum liquid layer. A summary of the highest energy barriers for the migration of Na and Al over all surfaces is presented in Table 2.

From above mentioned, the lower energy barriers of Na diffusion on TiB$_2$ surface suggests that the migration speed of sodium is larger than that of Al, and hence the deposited sodium will decrease the stability of Al layer and reduce the current efficiency of the cell. Besides, when the penetration of sodium occurs in the TiB$_2$ under the atmosphere of high temperature, the sodium diffusion inside TiB$_2$ is also the key factor for the potential application of TiB$_2$ as the cathode material in aluminum reduction cell, which determines the failure rate of TiB$_2$ during cell operation.

Bulk TiB$_2$ can be seen as a layered structure, including titanium metal sheet and hexagonal boron atom sheet along the c-axis [53], and diffusion of foreign atoms in this structure, such as Na and Al in bulk TiB$_2$, depends on the mobility of the point defects in the bulk. For bulk TiB$_2$, normally, there are three possible interstitial defect sites as shown in Fig. 4. Site1 and site2 represent the hollow sites of the Ti atoms and hexagonal boron atoms, respectively. Site3 is the center of the Ti2B2 polyhedron, as displayed in Fig. 4a. The both former interstitial defects with the corresponding high formation energies of 9.43, 12.74 eV for Na and 7.67, 9.8 eV for Al are difficult to form. Specially, for site3, this interstitial defect is not stability for Na and Al, the interstitial atom will move to Ti layer and occupy the bridge site of Ti atoms (Fig. 4a) and associated formation energies are 9.68 eV for Na, 7.4 eV for Al. This phenomenon also shows a strong covalent bond between Ti and B layers. Thus, the Na atom prefers to occupy the site1, while the Al atom prefers to occupy the site3. Not surprisingly, the high formation energies suggest that the TiB$_2$ bulk is a stable covalent crystal and the defects are difficult to form.

Then, to find the MEPs for Na and Al atoms diffusion in TiB$_2$, three

distinct pathways (Fig. 4b and Fig. S5)) were considered including the diffusion in Ti layer (path1), B layer (path3) and Ti-B interlayer (path2), respectively. As displayed in Fig. 4b, the Na diffusion of path1 will be from site1 to another site1, while Al migration from one site3 across a site1 to the next site3c. During the migration, the energy barriers of path1 are 0.23 and 0.26 eV for Na and Al, respectively. For the path2 (path3) (Fig. S5), hopping from site1 to site2 (from one site2 to another site2 for path3) requires overcoming large barriers for Na and Al. These values indicate that the diffusion of Na/Al may occur in Ti or B layers (path1 and path3) while the diffusion in interlayer (path2) is nearly impossible due to the large energy barriers. In short, the energy barriers are significantly larger than Na migration in graphite (0.29 eV), which implies the slower Na or Al penetration rate in TiB$_2$ than in graphite and this also is the advantage for TiB$_2$ cathode material compared to the current graphitized cathode materials.

3.4. Discussion

Usually, the Arrhenius equation, as shown in Eq. (1) [54], is adopted to express the relationship between diffusion coefficient and temperature.

$$D = D_0 \exp\left(-\frac{E_a}{k_B T}\right) \qquad (1)$$

where D_0, E_a, k_B and T represent the diffusion constant (pre-factor), energy barrier, Boltzmann constant and temperature. According to the transition state theory [55], the atomic diffusion rate can be exhibited as Eq. (2),

$$\mu = \nu \exp\left(-\frac{E_a}{k_B T}\right) \qquad (2)$$

in which, ν represents the atomic vibration frequency. Then, the D can be described as Eq. (3),

$$D = l^2 \nu \exp\left(-\frac{E_a}{k_B T}\right) \qquad (3)$$

where the l is the atomic transition distance. Furthermore, the ν can be obtained by the Wert-Zener theory [56], hence, the D can be calculated by the Eq. (4) [57], the m is the mass of diffusion atom.

$$D = l(E_a/2m)^{1/2} \exp\left(-\frac{E_a}{k_B T}\right) \qquad (4)$$

Based on the above equations, the diffusion coefficient of Na/Al on the TiB2 surface from 1000 K to 1400 K (determined by the electrolysis temperature) were shown in Fig. 5, which exhibits that the atomic diffusion coefficients of Na and Al diffusing at Ti-terminated surface are much larger than that at B-terminated surface or surfaces with Ti/B

Table 2
Summary of the highest diffusion energy barriers for the Na and Al migration on the pristine and the defective (V$_{Ti}$, V$_B$) TiB$_2$ surfaces.

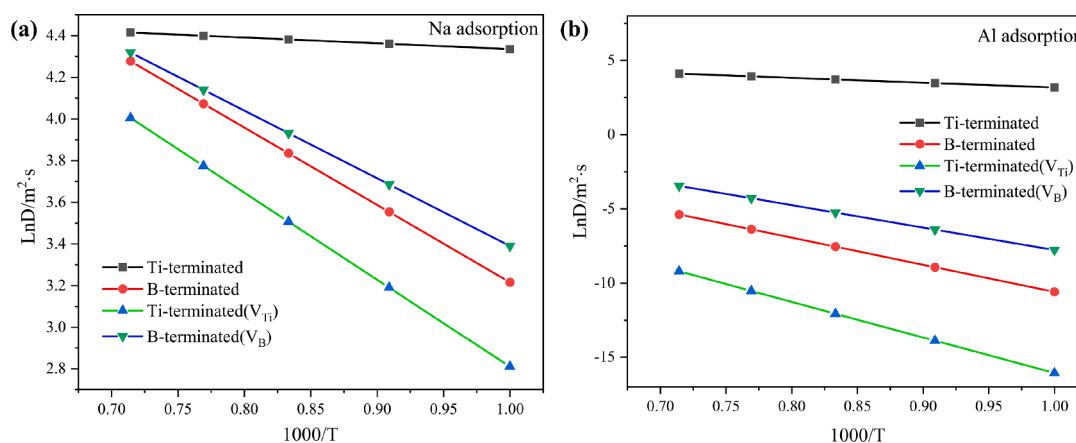| Adsorption atom	Diffusion energy barrier (eV)					
	Ti-terminated surface			B-terminated surface		
	pristine	V$_{Ti}$	V$_B$	pristine	V$_{Ti}$	V$_B$
Na	0.024	0.36	0.036	0.32	0.35	0.28
Al	0.28	2.07	0.32	1.57	1.66	1.3

Fig. 5. Relationship between LnD and temperature for (a) Na and (b) Al diffusion on different TiB2 surfaces.

vacancy. Obviously, this phenomenon is consistent well with the change of energy barrier, hence, the atomic diffusion coefficient will be determined by the distribution of potential energy surface on the TiB$_2$ surfaces, and the potential surface with the low energy barrier facilitates to atomic diffusion.

Due to the adaptation of cryolite electrolyte in aluminum reduction cell, the precipitation of sodium is unavoidable during the electrolysis process. From the above works, we know that the surface defects will increase the interaction between the precipitated sodium and TiB$_2$, promoting early process of permeation and shortening the service life of TiB$_2$. While, the inter property of perfect crystal will prevent the further permeation. In addition, the flater energy landscape (potential surface) of sodium above the TiB$_2$ surface will weaken the stability of aluminum liquid layer, which is detrimental to the improvement of current efficiency. Therefore, in terms of the cathode, for a better reduction cell, the novel cathode materials with the low sodium affinity should be developed, which can effectively prevent the initial process of the sodium permeation and decrease the possibility of the sodium corrision of the cathode surface. Specially, the experimental technique should be improved to obtain the perfect covalent crystal as the cathode material. Furthermore, the surface modification should be further studied to construct the high-barrier potential surface and limited the diffusion of sodium and aluminum.

4. Conclusion

Titanium diboride is the most suitable material for next-generation wettable cathode for aluminum reduction cell due to the perfect aluminum liquid wettability and the conductivity. However, the lack of understanding the mechanisms that causes the cathodes to fail, especially for the interaction of sodium with TiB$_2$, limits the development of the next-generation TiB$_2$ wettable cathode. By performing density functional theory calculations, we have analyzed the adsorption and diffusional characteristics of Na on TiB$_2$ surfaces and in TiB$_2$ crystal. Our investigations show that the adsorption energies of Na over the hollow sites of the Ti-terminate and B-terminated surfaces are −2.48 and −3.87 eV, respectively, which suggests the large possibility for sodium deposition on the TiB$_2$ surface, promotes the early process of permeation and may accelerate the failure of the TiB$_2$ material under Na-rich environment. Ti-vacant and B-vacant defects will enhance the adsorption stability and this tendency is more effective of V_{Ti} in Ti-terminal surface or V_B on B-terminal surface. The lower energy barriers of Na diffusion on TiB$_2$ surface than that of Al suggests that Na element will weaken the stability of aluminum liquid layer in the cathode of cell. Additionally, compare to graphite, the significantly higher energy barriers also reveal that Na and Al atoms have a much slower diffusion rate in TiB$_2$ crystal, so that the failure of TiB$_2$ is slower than graphite cathode under Na

environment. In general, the future study, for the industrialization of TiB$_2$ wettable cathode, should focus on the surface treatment to decrease the deposition of sodium and maintain the stability of aluminum liquid layer during the operation of aluminum reduction cell.

CRediT authorship contribution statement

Chaohong Guan: Conceptualization, Methodology, Investigation, Writing – original draft. **Hong Zhu:** Visualization, Supervision.

Declaration of Competing Interest

The authors declare that they have no known competing financial interests or personal relationships that could have appeared to influence the work reported in this paper.

Acknowledgements

Appendix A. Supplementary material

Supplementary data to this article can be found online at https://doi.org/10.1016/j.commatsci.2022.111535.

References:

[1] M. Soerlie, Cathodes in aluminium electrolysis, Aluminium 86 (2010) 102–103.
[2] R.P. Pawlek, Cathodes wettable by molten aluminum for aluminum electrolysis cells. 1990.
[3] J. Li, X.J. Lu, Y.Q. Lai, Q.Y. Li, Y.X. Liu, Research progress in TiB$_2$ wettable cathode for aluminum reduction, Cheminform 40 (2010) 32–37.
[4] C. Guan, X. Lv, Z. Han, C. Chen, The wetting characteristics of aluminum droplet on rough surfaces by molecular dynamics simulation, PCCP 22 (2020) 2361–2371.
[5] E. Yvenou, B. Davis, D. Guay, L. Roué, Electrodeposited TiB$_2$ on graphite as wettable cathode for Al production, J. Am. Ceram. Soc. 104 (2021) 1247–1254.
[6] J. Xue, Q. Liu, J. Zhu, W. Ou, Sodium penentration into carbon-based cathodes during aluminum electrolysis, TMS Light Met. 2006 (2006) 651–654.
[7] M. Pezzotta, Z.L. Zhang, M. Jensen, T. Grande, M.A. Einarsrud, Cohesive zone modeling of grain boundary microcracking induced by thermal anisotropy in titanium diboride ceramics, Comput. Mater. Sci. 43 (3) (2008) 440–449.
[8] Y. Mikhalev, H.A. Oye, Absorption of metallic sodium in carbon cathode materials, Carbon 34 (1) (1996) 37–41.
[9] C. Schøning, T. Grande, O.-J. Siljan, Cathode Refractory Materials for Aluminium Reduction Cells, in: A. Tomsett, J. Johnson (Eds.), Essential Readings in Light Metals, Springer International Publishing, Cham, 2016, pp. 849–856.
[10] C.H. Clelland, J.T. Keniry, B.J. Welch, Influence of Cell Operation on Cathode Life in Aluminum Reduction, J. Met. 34 (2013) 54–58.
[11] K. Grjotheim, Aluminium Electrolysis: Fundamentals of the Hall-Heroult Process (1982).

[12] R. Pelletier, C. Allaire, Corrosion in potlining refractories: Effect of cathode material interpreted using a unified approach, JOM 55 (11) (2003) 58–62.

[13] T. Min, L. Tao, B. Yza, S.D. Bo, D. Jie, Study on the dissolution of aluminium carbide formed on the graphite cathode in aluminium electrolysis, J. Mol. Liq. 331 (2021), 115767.

[14] Z. Fang, K. Zhang, X. Lü, L.B. Li, J. Zhu, J. Li, Alkali metals (K and Na) penetration and its effects on expansion of TiB2-C composite cathode during aluminum electrolysis, Trans. Nonferrous Met. Soc. China 23 (2013) 1847–1853.

[15] J.G. Hooley, P.T. Hough, Intercalation properties of the carbon cathode of aluminum reduction cells, Carbon 16 (1978) 221–223.

[16] A. Zolochevsky, J.G. Hop, T. Foosnaes, H.A. Oye, Surface exchange of sodium, anisotropy of diffusion and diffusional creep in carbon cathode materials, Light Met. (2005) 745–750.

[17] A. Hérold, J. Marêché, M. Lelaurain, Intercalation of sodium with its halides into graphite, Carbon 38 (2000) 1955–1963.

[18] P. Brilloit, L.P. Lossius, H. Øye, Penetration and chemical reactions in carbon cathodes during aluminum electrolysis: part i. laboratory experiments, Metall. Trans. B 24 (1993) 75–89.

[19] E. Matuyama, Successive Stages of a Graphite-Potassium Compound and its Thermal Expansion, Nature 193 (1962), 61–61.

[20] N. Adhoum, J. Bouteillon, D. Dumas, J.C. Poignet, Electrochemical insertion of sodium into graphite in molten sodium fluoride at 1025 °C, Electrochim. Acta 51 (25) (2006) 5402–5406.

[21] B. Chan, K.M. Thomas, H. Marsh, The interactions of carbons with potassium, Carbon 31 (7) (1993) 1071–1082.

[22] P.Y. Brisson, H. Darmstadt, M. Fafard, A. Adnot, G. Servant, G. Soucy, X-ray photoelectron spectroscopy study of sodium reactions in carbon cathode blocks of aluminium oxide reduction cells, Carbon 44 (8) (2006) 1438–1447.

[23] J. Xue, H.A. Ye, Sodium and Bath Penetration into TiB 2 -Carbon Cathodes during Laboratory Aluminium Electrolysis, Essential Readings Light Met. (2016).

[24] Z. Wang, J. Friis, A.P. Ratvik, Transport of Sodium in TiB2 Materials Investigated by a Laboratory Test and DFT Calculations, Light Metals (2018).

[25] S. Yang, S. Li, S. Tang, D. Shen, W. Dong, W. Sun, Adsorption, intercalation and diffusion of Na on defective bilayer graphene: a computational study, Surf. Sci. 658 (2017) 31–37.

[26] O.I. Malyi, K. Sopiha, V.V. Kulish, T.L. Tan, S. Manzhos, C. Persson, A computational study of Na behavior on graphene, Appl. Surf. Sci. 333 (2015) 235–243.

[27] X. Fan, W.T. Zheng, J.-L. Kuo, Adsorption and Diffusion of Li on Pristine and Defective Graphene, ACS Appl. Mater. Interfaces 4 (5) (2012) 2432–2438.

[28] D. Datta, J. Li, V.B. Shenoy, Defective graphene as a high-capacity anode material for Na- and Ca-ion batteries, ACS Appl. Mater. Interfaces 6 (3) (2014) 1788–1795.

[29] H. Yildirim, A. Kinaci, Z.-J. Zhao, M.K.Y. Chan, J.P. Greeley, First-Principles Analysis of Defect-Mediated Li Adsorption on Graphene, ACS Appl. Mater. Interfaces 6 (23) (2014) 21141–21150.

[30] C. Biz, M. Fianchini, V. Polo, J. Gracia, Magnetism and Heterogeneous Catalysis. In Depth on the Quantum Spin-Exchange Interactions in Pt 3 M (M = V, Cr, Mn, Fe Co, Ni, and Y)(111) Alloys, ACS Appl. Mater. Interfaces 12 (45) (2020) 50484–50494.

[31] J.P. Perdew, K. Burke, M. Ernzerhof, Generalized Gradient Approximation Made Simple, Phys. Rev. Lett. 77 (18) (1998) 3865–3868.

[32] Sian A. Joyce, Jonathan R. Yates, Chris J. Pickard, S.P. Brown, Density Functional Theory Calculations of Hydrogen-Bond-Mediated NMRJCoupling in the Solid State, J. Am. Chem. Soc. 130 (38) (2008) 12663–12670.

[33] Naoki; Imamura; Hiroshi; Mizoguchi; Hideo; Hosono, Superconductivity in LaTMBN and La3TM2B2N3 (TM = Transition Metal) Synthesized under High Pressure, J. Am. Chem. Soc. 134 (5) (2012) 2516–2519.

[34] Z. Ao, Q. Jiang, S. Li, H. Liu, F.M. Peeters, S. Li, G. Wang, Enhancement of the Stability of Fluorine Atoms on Defective Graphene and at Graphene/ Fluorographene Interface, Mater. Interfaces 7 (35) (2015) 19659–19665.

[35] D.J. Chadi, Special points for Brillouin-zone integrations, Phys. Rev. B 16 (4) (1977) 1746–1747.

[36] S. Grimme, Semiempirical GGA-type density functional constructed with a long-range dispersion correction, J. Comput. Chem. 27 (15) (2006) 1787–1799.

[37] Q. Meng, J. Ma, Y. Zhang, L. Zhen, H.U. Alice, J.J. Kai, J. Fan, Theoretical investigation of zirconium carbide MXenes as prospective high capacity anode materials for Na-ion batteries, J. Mater. Chem. A 6 (2018) 13652–13660.

[38] S. Mukherjee, L. Kavalsky, C.V. Singh, Ultrahigh Storage and Fast Diffusion of Na and K in Blue Phosphorene Anodes, ACS Appl. Mater. Interfaces 10 (10) (2018) 8630–8639.

[39] J.S. Jirkovsky, M. Busch, E. Ahlberg, I. Panas, P. Krtil, Switching on the electrocatalytic ethene epoxidation on nanocrystalline RuO2, J. Am. Chem. Soc. 133 (15) (2011) 5882–5892.

[40] Z. Jiao, Q.J. Liu, F.S. Liu, B. Tan, Structural and electronic properties of low-index surfaces of NbAlintermetallic with first-principles calculations, Appl. Surf. Sci. 419 (2017) 811–816.

[41] Q. Wang, C. Liu, R. Yao, H. Zhu, H. Wang, First-principles study on the stability and work function of low-index surfaces of TiB$_2$, Comput. Mater. Sci. 172 (2019), 109356.

[42] J.K. Burdett, E. Canadell, G.J. Miller, Electronic structure of transition-metal borides with the AlB$_2$ structure, J. Am. Chem. Soc. 108 (21) (1986) 6561–6568.

[43] L. Topor, O.J. Kleppa, Enthalpies of formation of first-row transition-metal diborides by a new calorimetric method, J. Chem. Thermodyn. 17 (11) (1985) 1003–1016.

[44] Q. Wang, Y. Li, S. Chen, X. Liu, Z. Chen, M. Wang, H. Zhu, H. Wang, Interface Alloying Design to Improve the Dispersion of TiB$_2$ Nanoparticles in Al Composites: A First-Principles Study, J. Phys. Chem. C 125 (10) (2021) 5937–5946.

[45] Y. Ma, A. Addad, G. Ji, M.X. Zhang, V. Ji, Atomic-scale investigation of the interface precipitation in a TiB2 nanoparticles reinforced Al-Zn-Mg-Cu matrix composite, Acta Mater. 185 (2019) 287–299.

[46] R. Liu, X. Yin, K. Feng, R. Xu, First-principles calculations on Mg/TiB$_2$ interfaces, Comput. Mater. Sci. 149 (2018) 373–378.

[47] V. Ilyasov, G.B. Long, A.V. Ilyasov, T.P. Zhdanova, G.A. Geguzina, H.V. Phuc, N. N. Hieu, C.V. Nguyen, K.D. Pham, First-principles study of W, N, and O adsorption on TiB$_2$(0001) surface with disordered vacancies, Superlattices Microstruct. 123 (2018) 414–426.

[48] L.H. Yao, M.S. Cao, H.J. Yang, X.J. Liu, X.Y. Fang, J. Yuan, Adsorption of Na on intrinsic, B-doped, N-doped and vacancy graphenes: A first-principles study, Comput. Mater. Sci. 85 (2014) 179–185.

[49] X. Sun, Z. Wang, Y.Q. Fu, Adsorption and diffusion of sodium on graphene with grain boundaries, Carbon 116 (2017) 415–421.

[50] X. Kang, J. Xiang, Y. Lv, W. Du, H. Yu, S. Wang, M. Zhu, Synthesis and Structure of Self-Assembled Pd$_2$Au$_{23}$(PPh$_3$)$_{10}$Br 7 Nanocluster: Exploiting Factors That Promote Assembly of Icosahedral Nano-Building-Blocks, Chem. Mater. 29 (16) (2017) 6856–6862.

[51] S. Mukherjee, A. Banwait, S. Grixti, N.A. Koratkar, C.V. Singh, Adsorption and Diffusion of Lithium and Sodium on Defective Rhenium Disulfide: A First Principles Study, ACS Appl. Mater. Interfaces (2018) 5373–5384.

[52] R. Zhang, X. Wu, J. Yang, Block of Ultrafast and Directional Diffusion of Li on Phosphorene with Intrinsic Defects, Nanoscale 8 (7) (2016) 4001–4006.

[53] C. Li, X. Liu, L. Zhu, R. Huang, M. Zhao, L. Xu, Y. Qian, Conductive and Polar Titanium Boride as a Sulfur Host for Advanced Lithium-Sulfur Batteries, Chem. Mater. 30 (20) (2018) 6969–6977.

[54] S. Arrhenius, Über die Reaktionsgeschwindigkeit bei der Inversion von Rohrzucker durch Säuren, Z. Phys. Chem. 4 (1889) 226–248.

[55] G.H. Vineyard, Frequency factors and isotope effects in solid state rate processes, J. Phys. Chem. Solids 3 (1957) 121–127.

[56] C. Wert, C. Zener, Interstitial atomic diffusion coefficients, Phys. Rev. B 76 (1949) 1169–1175.

[57] L. Chao, Y. Jian, L. Xuanwei, H. Jihua, Y. Zheng, C. Shuhai, Z. Yue, First-principle calculations on adsorption-diffusion behavior of Boron atom with tungsten surface, Comp. Mater. Sci. 183 (2020), 109908.